Interdiffusion and self-diffusion in polymer mixtures: A Monte Carlo study

Cite as: J. Chem. Phys. **94**, 2294 (1991); https://doi.org/10.1063/1.459901
Submitted: 06 September 1990 . Accepted: 04 October 1990 . Published Online: 31 August 1998

H. P. Deutsch, and K. Binder

Interdiffusion and self-diffusion in polymer mixtures: A Monte Carlo study

H. P. Deutsch and K. Binder
Institut für Physik, Johannes-Gutenberg-Universität Mainz, Staudinger Weg 7, D-6500 Mainz, Federal Republic of Germany

(Received 6 September 1990; accepted 4 October 1990)

A lattice model for dense polymer solutions and polymer mixtures in three dimensions is presented, aiming to develop a model suitable for efficient computer simulation on vector processors, with a qualitatively realistic local dynamics. It is shown that the bond fluctuation algorithm for a suitable set of allowed bond vectors has the property that due to the excluded volume constraint no crossing of bonds by local motions can occur, and entanglement restrictions thus are fully taken into account. For athermal binary (AB) symmetrical polymer mixtures, the dependence of both self-diffusion coefficient and interdiffusion coefficient on polymer density is obtained, simulating a thin film geometry where a film of polymer A is coated with a film of polymer B. For one density, the dependence of the interdiffusion coefficient on an attractive energy between unlike monomers is also studied. For weak attraction an enhancement of interdiffusion proportional to this energy occurs. For strong attraction, however, a rather immobile tightly bound AB layer forms in the interface which hampers further unmixing.

I. INTRODUCTION AND OVERVIEW

Dense systems of long flexible macromolecules exhibit motions on time scales ranging over many orders of magnitude, and despite impressive progress of the theory of polymer dynamics[1] many aspects of these motions are incompletely understood. Thus there has been a longstanding interest to clarify some of these problems by computer simulations.[2-4] Since the large range of time scales of these motions makes it impossible to equilibrate realistic models of long polymer chains even on today's fastest computers,[4] choice of coarse-grained models of the polymers (where information on the detailed chemical structure on the monomer length scale is omitted) is inevitable if one insists to work with reasonably well equilibrated chains. Both models in continuum space (such as the pearl-necklace model[2,5] and the bead–spring model with Lennard-Jones interaction[6]) and lattice models[3,7-13] have therefore been considered. While both the Monte Carlo[5] and the molecular dynamics[6] simulations of such off-lattice models yield very promising results, the requirements in computing time still are rather large, and thus the use of slightly less realistic lattice models still is of interest. There is a considerable freedom in the "invention" of such a model.[3] For dynamical properties of dense polymers, however, a sensible model should satisfy the following criteria: (i) The elementary motion should be a random local move [or a set of such moves, cf. Fig. 1(a)], in order that on small scales in space and time the Rouse model dynamics[1,14] is reproduced. (ii) The "effective monomers" must not overlap to simulate the excluded-volume interaction among the chains. (iii) During the motions there must not be any bond intersection, in order to simulate the entanglement restrictions on the dynamics.[1,15] (iv) The algorithm should be ergodic (i.e., all configurations of the phase space should be accessible).[9]

The most popular choice of lattice model is a generalization of the Verdier–Stockmayer[7] model, where the polymer is represented by a self-avoiding walk (SAW) on a simple cubic lattice, and at least the three types of motions shown in Fig. 1(a) are permitted. However, this model has several drawbacks: it is not useful in two dimensions since there all motions in the chain interior conserve the bond vectors;[12] for rather short chains one has already "forbidden" configurations which can neither be reached nor be relaxed with this algorithm.[9] The fact that the ergodicity of this algorithm may be a problem is also obvious from the fact that the motions in Fig. 1(a) cannot translate the chain by one lattice unit on the lattice. Since each bond of the SAW should physically correspond to a "Kuhn segment" formed by several successive chemical monomers, it is also undesirable to have only two choices for the value of the angle between two successive bonds of the SAW (0°, $\pm 90°$).

Thus, we use an alternative algorithm following a recent proposal by Carmesin and Kremer.[12] In this bond fluctuation algorithm, one constructs a chain as indicated in Fig. 1(b). In the center of an effective monomer, eight neighboring lattice sites (on the corner of a cube) are all blocked for occupation by other monomers, to model excluded volume constraints. The bond vector $\mathbf{l}$ connecting two successive effective monomers may have lengths in the range $l_{\min} \leqslant l \leqslant l_{\max}$. This fluctuation in the length of the bond vector can be thought of to correspond to the fluctuation in the length of the physical "Kuhn segment," the latter being due to the fact that the sequence of chemical segments which form the Kuhn segment may take on many different conformations. It is sufficient to consider one type of move, namely the random jump of an effective monomer in a randomly chosen lattice direction by a lattice unit. This trial motion in the Monte Carlo algorithm is accepted only if neither the excluded volume constraint is violated nor the restriction on the allowed range of the bond length. Obviously, the two bonds joining at the moving effective monomer get new bond vectors when the move is accepted, with different lengths. This dynamics is thought to be physically caused by random conformational changes of the chemical monomers which

 0021-9606/91/032294-11$03.00

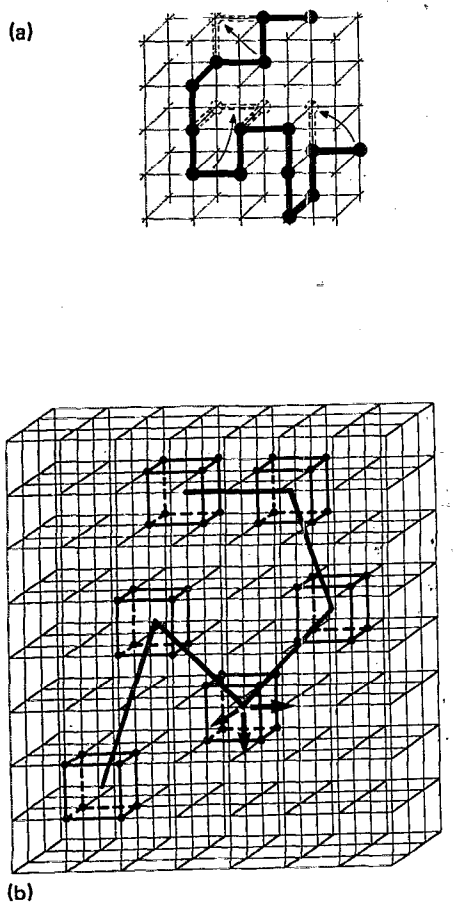

FIG. 1. (a) Schematic illustration of the standard Verdier–Stockmayer-type lattice model for the simulation of polymer dynamics. Chains are modeled as self- and mutually avoiding random walks. Chain configurations relax by a set of random motions (end rotation, 90° crankshaft rotation, and kink jump motion, for instance). (b) Schematic illustration of the bond fluctuation model. An effective monomer blocks a cube containing eight lattice sites for occupation by other monomers. The length of the bonds connecting two neighboring cubes along the chain must lie in the interval $l_{\min} \leqslant l \leqslant l_{\max}$. Chain configurations relax by random diffusive hops of the effective monomers (e.g., these hops may be restricted to one lattice spacing in lattice directions, as indicated by the arrows).

form one effective unit. A further advantage of this algorithm is that it is also useful for branch points in polymer networks or star polymers.

This algorithm has before been used mainly in two space dimensions[12] where the standard algorithm of Fig. 1(a) would fail to reproduce the dynamics of the Rouse model[14] even for a single chain.[3] In a previous application[13] in $d = 3$ dimensions, the intersection of chains in the course of a sequence of motions as shown in Fig. 1(b) was not forbidden; such an unrealistic choice of dynamics is avoided in the present work.

In Sec. II, it is shown that there exists a set of allowed bond vectors for which the excluded volume constraint automatically ensures that bonds cannot intersect, and entanglement restrictions hence can be taken into account in a very simple manner. Also variants of the model are studied where monomers are allowed to hop over distances larger than nearest neighbor. It is shown that the simple choice of Fig. 1(b) is preferable since it actually gives rise to faster diffusion than the dynamics with these larger jump distances.

After this investigation of the method, we present applications to the problem of interdiffusion in polymer blends, a problem which has found a lot of attention both theoretically[13,16–30] and experimentally.[16,17,31–40] Although it has become clear[16,17,26] that the lattice model disregards an important aspect of this problem, namely hydrodynamic flow mechanisms of interdiffusion, it is nevertheless of interest to clarify the behavior in the limit where such hydrodynamic effects are absent. Section III presents some new results on the behavior of both self-diffusion and interdiffusion as a function of polymer density in an "ideal" polymer mixture, where apart from excluded volume there is no interaction between A and B monomers in the (AB) mixture. In Sec. IV the dependence of the interdiffusion constant on the interaction parameter describing an attractive interaction between monomers of different kind in compatible mixtures is studied and compared to theoretical predictions. Section V contains some concluding remarks.

II. THE BOND FLUCTUATION METHOD IN THREE DIMENSIONS

As mentioned above, we want to define an algorithm based on the model shown in Fig. 1(b), which not only is consistent with the excluded volume interaction between the effective monomers, but where also the chains formed by connecting the centers of gravity of the effective monomers cannot intersect each other in the course of their random motions. Here we show that this condition can be automatically satisfied by a suitable restriction on the set of bond vectors $\{\mathbf{b}\} = \{\Delta x, \Delta y, \Delta z\}$ connecting two successive monomers. This set must be a *connected set* where we use this term in the sense that for a pair of effective monomers each bond vector $\mathbf{b}$ of the set can be reached from each other bond vector $\mathbf{b}'$ belonging to the set via a succession of the elementary motions possible for the effective monomers. Choosing the lattice spacing as unity, these elementary motions in the case of Fig. 1(b) are

$$\{\Delta b\} = \boldsymbol{P}(1,0,0). \tag{1}$$

where $\mathbf{P}(\Delta x, \Delta y, \Delta z)$ stands for the set of all permutations and sign combinations of $\pm \Delta x$, $\pm \Delta y$, $\pm \Delta z$. Our assertion then is that the set of bonds $\mathbf{B}$,

$$\mathbf{B} = \mathbf{P}(2,0,0) \cup \mathbf{P}(2,1,0) \cup \mathbf{P}(2,1,1) \cup \mathbf{P}(2,2,1) \cup \mathbf{P}(3,0,0) \cup \mathbf{P}(3,1,0) \tag{2}$$

has the desired property that the chains formed by bonds from this set cannot cross, while if we would include longer bonds the chain would behave as "phantom chains" where bonds are cut in the course of their motions.

From Eq. (2) we immediately see that this set contains 108 bonds with five different choices of the bond length $b = |\mathbf{b}|$:

$$b = 2, \sqrt{5}, \sqrt{6}, 3\sqrt{10}. \tag{3}$$

Two successive bonds may have 87 different bond angles ϑ in the interval $[0,\pi]$. Figure 2 shows the "*a priori* probability" distribution $P(\vartheta)$ of the bond angle. By *a priori* probability we mean a probability constructed not for a long chain (where the excluded-volume interaction introduces also

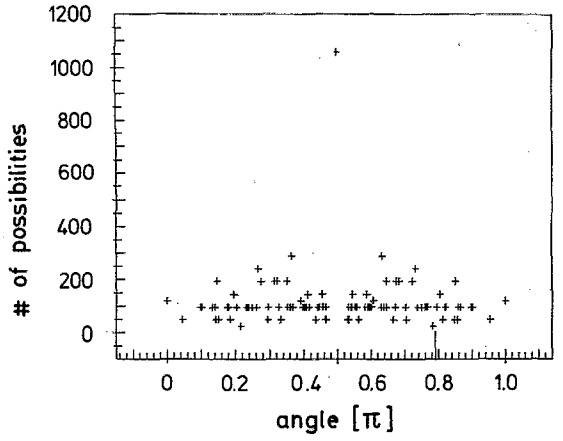

FIG. 2. Number of possibilities for the angle ϑ between two successive bonds in the bond fluctuation model as defined by Eqs. (2) and (3) and illustrated in Fig. 1. The angle is measured in units of π and $\vartheta = 0$ means that the two bond vectors are oriented along the same direction. Note that all angles to the right of the vertical bar near $\vartheta/\pi = 0.8$ are forbidden due to excluded volume constraints.

orientational correlations for the bond vectors along the chain) but for a chain consisting of two bonds only. It is seen that this probability has a sharp maximum at $\vartheta_{\max} = \pi/2$, and is symmetric around this value apart from the fact that very large angles do not occur, because already for two bonds the excluded volume interaction forbids a too sharp reversal of the second bond relative to the first. While the model of Fig. 1(a) would have only the two distinct entries $\vartheta = 0, \pi/2$ in this distribution, the spectrum of bond angles for the present model is very rich! Of course, the lattice structure still shows up in $P(\vartheta)$ in terms of the obvious oscillatory structure. If one computes $P(\vartheta)$ for Kuhn segments of a realistic model of real polymers such as polyethylene, a rather smooth distribution $P(\vartheta)$ is in fact obtained.[41] For a comparison of $P(\vartheta)$ to real polymers one thus needs to average $P(\vartheta)$ over an angular interval $\Delta\vartheta$ distinctly larger than the distance between successive possible angles in Fig. 2 in order to somewhat reduce these lattice artefacts.

Now we discuss the argument which leads us to Eq. (2). By inspection of possible motions one readily finds that bond intersection is possible if any coordinate difference Δx, Δy, or Δz would be equal or larger than 4. Eliminating such bond vectors with $\Delta x \geqslant 4$ (or $\Delta y \geqslant 4$, $\Delta z \geqslant 4$), it is useful to split the set of two remaining bond vectors into two subsets:

$$\mathbf{B}_1 = \mathbf{P}(2,0,0) \cup \mathbf{P}(2,1,0) \cup \mathbf{P}(2,1,1) \cup \mathbf{P}(3,0,0), \tag{4}$$

$$\mathbf{B}_2 = \mathbf{P}(2,2,0) \cup \mathbf{P}(2,2,1) \cup \mathbf{P}(2,2,2) \cup \mathbf{P}(3,1,0) \cup \mathbf{P}(3,1,1) \cup \mathbf{P}(3,2,0) \cup \mathbf{P}(3,2,1) \cup \mathbf{P}(3,2,2) \cup \mathbf{P}(3,3,0) \cup \mathbf{P}(3,3,1) \cup \mathbf{P}(3,3,2) \cup \mathbf{P}(3,3,3). \tag{5}$$

By inspection one realizes that the set of bonds $\mathbf{B}_1$ is permitted, since these bond vectors are so short that for any configuration where bonds intersect the effective monomers would overlap. This is not true for the bond vectors from the set $\mathbf{B}_2$, however: e.g., the bond vectors (2,2,0) and (2, −2,0) can cross without violating the excluded volume constraint for the effective monomers. However, nevertheless one can choose some bond vectors from the set $\mathbf{B}_2$ if one ensures that the dynamics of the model is suitably restricted such that configurations with intersecting bonds cannot be reached from allowed configurations. This condition for the restricted set $\mathbf{B}_2'$ is ensured if we require that only such bond vectors of the set $\mathbf{B}_2$ are included in $\mathbf{B}_2'$ which satisfy the condition that each bond vector of $\mathbf{B}_2'$ is connected with *one* elementary move $\Delta\mathbf{b}$ [Eq. (1)] only to a bond vector of the set $\mathbf{B}_1$, but not to another vector of the set $\mathbf{B}_2'$. Omitting thus from $\mathbf{B}_2$ all vectors which are not connected with one elementary move to any vector of $\mathbf{B}_1$ immediately yields the restricted set

$$\mathbf{P}(2,2,0) \cup \mathbf{P}(2,2,1) \cup \mathbf{P}(3,1,0) \cup \mathbf{P}(3,1,1). \tag{6}$$

Since both $\mathbf{P}(2,2,0)$ is connected with one elementary move to $\mathbf{P}(2,2,1)$ and $\mathbf{P}(3,1,0)$ to $\mathbf{P}(3,1,1)$, a further restriction is necessary, omitting two types of bond vectors out of the four types kept in Eq. (6). This restriction is not unique: one could choose $\mathbf{B}_2' = \mathbf{P}(2,2,0) \cup \mathbf{P}(3,1,0)$ or $\mathbf{B}_2' = \mathbf{P}(2,2,0) \cup \mathbf{P}(3,1,1)$ or $\mathbf{B}_2' = \mathbf{P}(2,2,1) \cup \mathbf{P}(3,1,1)$ or

$$\mathbf{B}_2' = \mathbf{P}(2,2,1) \cup \mathbf{P}(3,1,0), \tag{7}$$

which is the choice we have taken. The motivation for this choice was that $\mathbf{P}(2,2,1)$ contains more bonds than $\mathbf{P}(2,2,0)$ and that the bonds of $\mathbf{P}(3,1,0)$ are shorter than those of $\mathbf{P}(3,1,1)$. Combining Eqs. (4) and (7) then immediately yields Eq. (2). Although this choice may seem arbitrary, we note in its favor that we keep *all* bonds in the range from $l_{\min} = 2$ to $l_{\max} = \sqrt{10}$ with the exception of $\mathbf{P}(2,2,0)$: if we would allow those as well, chains could intersect. Thus our choice is motivated by the desire to keep as many bond vectors as possible and at the same time restrict the chosen interval of bond lengths as little as possible. By including many bond vectors from the set $\mathbf{B}_2'$, dense configurations of many-chain systems have much more possibilities for ongoing monomer motions, and hence a much quicker relaxation towards equilibrium may be anticipated.

In the course of the stochastic Monte Carlo process generated by a succession of motions with displacements randomly chosen from Eq. (1), a considered bond vector can stay inside of the set $\mathbf{B}_1$, or it can make a transition to the set $\mathbf{B}_2'$. If this happens, a change at the next time step must lead back to the set $\mathbf{B}_1$. The fact that for two pairs of bonds in the set $\mathbf{B}_2'$ both their previous generation and their next generation (in the course of their "time" evolution) must belong to $\mathbf{B}_1$ ensures that the effective monomers cannot move in such a way where an intersection of bonds would occur.

Of course, it is straightforward to include effects due to a finite interaction energy into this algorithm. We simply have to consider the (Metropolis)[2-4,43] transition probability w,

$$w = \min[1, \exp(-\Delta E/k_B T)] \tag{8}$$

for accepting or rejecting a move, which is allowed according to the excluded volume and bond vector restrictions, but involves an energy change ΔE. In the definition of the pairwise energy between effective monomers, there is also a certain freedom in the choice of the center of the potential. We work with an energy ϵ between pairs of monomers, their distance vector from center to center is either $\mathbf{P}(2,0,0)$, $\mathbf{P}(2,1,0)$, or $\mathbf{P}(2,1,1)$. To define the position of a monomer

on the lattice, the lower, left, front corner of the monomer cube [Fig. 1(b)] is chosen. Around a considered monomer position thus 54 neighbor sites need to be checked for occupancy due to neighboring effective monomers, while for the model of Fig. 1(a) the standard choice involves only six nearest neighbor sites.[2-4,44,45] At this point, in the present algorithm considerably more computation is involved. The reason for including so many neighbor sites is that we wish to include all sites which contribute to the first peak of the radial density distribution function in dense polymer systems in our model (Fig. 3). The maximum number of different effective monomers with which one effective monomer may interact is 14 (for an inner monomer of a chain at least two of these monomers must belong to the same chain, of course). For our consideration of binary polymer blends, we only introduce an attractive energy ϵ_{AB} between monomers belonging to different types of chain, but energies between monomers of the same kind are set equal to zero. Such energies ϵ_{AA}, ϵ_{BB} would already significantly affect the configuration of a single chain in our model, because for the two shortest bond vectors these energies would contribute an intrachain interaction along the backbone of the chain.

When one compares the dynamical properties of the present algorithm to that of Fig. 1(a), it should be noted that Fig. 1(a) involves a random choice between different types of motion, while the present algorithm allows only a single type. This latter feature, of course, is desirable for a fast performance of the algorithm. Another difference is that the jump distance of an effective monomer in Fig. 1(a) is equal to the distance between the effective monomers, while in Fig. 1(b) it is distinctly smaller. Considering that the center of gravity of a Kuhn segment moves due to random conformational changes of the chemical monomers contained in the segment, the present choice clearly is a bit closer to physical reality. On the other hand, one might argue that a quicker relaxation towards equilibrium is obtained, if the monomers could jump a larger distance in a single step.

In order to test this point in the framework of our algorithm, we have considered two variants where instead of Eq. (1) also jumps in diagonal directions are included:

$$\{\Delta b'\} = \mathbf{P}(1,0,0) \cup \mathbf{P}(1,1,0), \tag{9}$$

$$\{\Delta b''\} = \mathbf{P}(1,0,0) \cup \mathbf{P}(1,1,0) \cup \mathbf{P}(1,1,1). \tag{10}$$

While according to Eq. (1) a monomer has six *a priori* choices for the jump, it has 18 for the choice Eq. (9) and 26 for the choice Eq. (10). In the case of Eqs. (9) and (10), one must restrict the choice of bond vectors to the set $\mathbf{B}_1$ [Eq. (4)], to avoid the intersection of bonds, however,

In Fig. 4 we now compare typical results for the mean square center of mass displacement of short chains for two typical cases, using the three algorithms [Eqs. (1), (9), and (10)] [for $\phi = 0.05$ we here also use the restricted set $\mathbf{B}_1$ of bond vectors for the choice of Eq. (1), unlike the rest of this paper, for the sake of comparison]. Although the new motions involve larger jump distances ($\sqrt{2}$ and $\sqrt{3}$ instead of unity, respectively), it is seen that even in the dilute limit the diffusion of the chains is not speeded up by the use of Eq. (9)

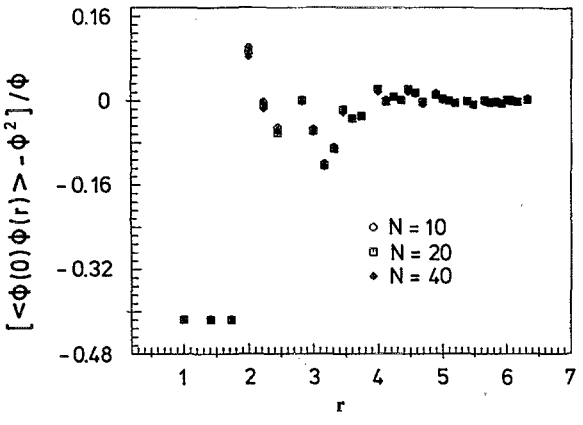

FIG. 3. Radial monomer density distribution function around an effective monomer of a polymer chain plotted vs distance for several chain lengths N at average volume fraction $\phi = 0.42$. Note that the values for which $g(R) = -\phi$ correspond to distances between monomers which are forbidden because of excluded volume constraints. All lengths are measured in units of the lattice spacing.

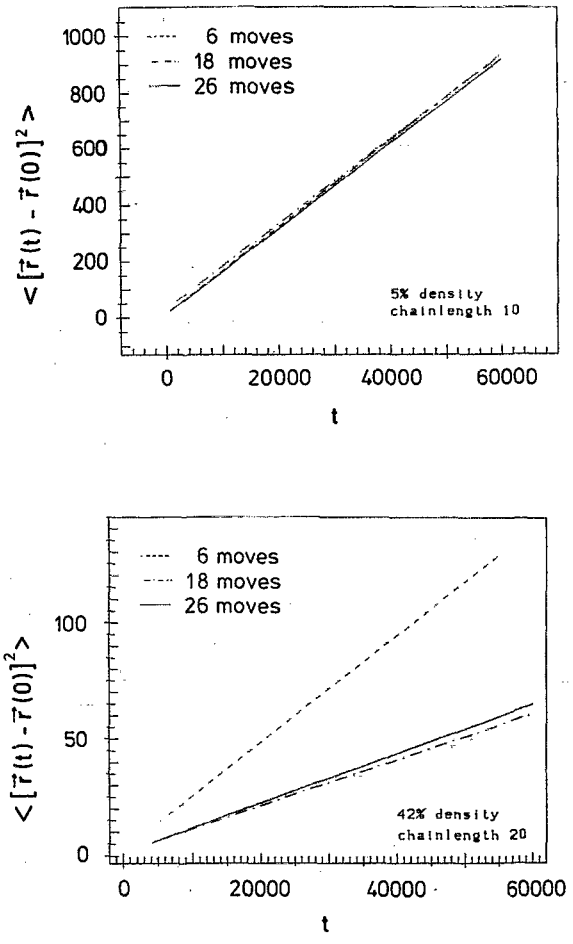

FIG. 4. Mean square center of mass displacement plotted vs simulation time (in the unit of attempted Monte Carlo steps per monomer). Case (a) refers to a system at a volume fraction $\phi = 0.05$ of lattice sites being part of effective monomers, chain length $N = 10$, while case (b) refers to a system of $\phi = 0.50$, $N = 20$. Full, broken, and dash–dotted curves show the behavior for the choice of jump distances according to Eqs. (1), (9), and (10), respectively. Both cases refer to an athermal situation.

or (10), respectively, and for concentrated systems the choice Eq. (1) actually is the fastest! This observation is readily understood, of course, by noting that the acceptance rate for a move strongly goes down with increasing jump distance, due to the constraint that one must not leave the set $\mathbf{B}_1$ of allowed bond vectors. For a dilute system, the decrease of the average acceptance rate and the increase of the mean square displacement per accepted jump just happen to nearly cancel if always the set $\mathbf{B}_1$ is chosen; for dense systems, the excluded volume condition is more likely violated the larger the jump distance, and this fact further lowers the acceptance rate. Direct "measurements" of the respective acceptance rates for the various types of jumps support these conclusions.[46]

In summary, our algorithm is fairly robust against changes of detail (Fig. 3), and the choice defined in Eqs. (1) and (2) is also preferable from the point of view of an economic use of computer time.

III. SELF-DIFFUSION VS INTERDIFFUSION IN IDEAL SYMMETRIC NONINTERACTING POLYMER MIXTURES

As a first application of this algorithm, we study further the idea expressed widely in the literature[16–28] that there exists a simple relation by which the interdiffusion coefficient of a mixture can be expressed in terms of the self-diffusion coefficients of of the two constituents. This idea has been cast into doubt both by more recent elaborate theories[29] and by simulations of lattice gases[30] and polymer mixtures[13] where the jump rates of the two types of monomers differed. While previous work[13] was mainly concerned with an attempt to distinguish between the "fast mode" theory (faster diffusing species controls interdiffusion[21,22,25]) and the "slow mode" theory (slower diffusing species controls interdiffusion[18–20,23,24,26,27]), here we test a case where both these theories would yield an identical result. This occurs for the special case where both the volume fractions ϕ_A, ϕ_B of the two monomer species and their self-diffusion constants D_A, D_B are equal, $\phi_A = \phi_B = \phi/2, D_A = D_B = D$. Then all these theories[16–27] simply imply

$$D_{\text{int}} = D_{\text{self}}. \tag{11}$$

Of course, Eq. (11) is a kind of mean-field result where correlation effects are neglected. As is well known for the problem of diffusion in crystals,[30,47–50] where diffusion is mediated by vacancies, there are complicated dynamic correlations introduced due to the enhanced backjump probability to a vacant site. Therefore the actual diffusion constant is reduced by a "correlation factor"[47–50] in comparison to the corresponding mean field prediction. In general, different correlation factors apply for D_{int} and D_{self}, and thus Eq. (11) no longer is expected to be valid. While Monte Carlo evidence for simple lattice gas models[30] shows that there Eq. (11) is inaccurate, a systematic test of Eq. (11) for polymer mixtures has not yet been performed. One might expect that in fluid polymer mixtures the diffusion of "free volume" may lead to similar dynamic correlations as the vacancy diffusion in crystals.

Our numerical estimation of D_{int} and D_{self} closely follow the techniques described in Ref. 13 and thus only the main points are summarized. We choose a geometry of $20\times20\times80$ for the simple cubic lattice, with two free 20×20 surfaces with a "hard wall" boundary condition and periodic boundary conditions in the two remaining directions. This particular geometry is convenient for the study of interdiffusion via the broadening of concentration profiles:[13] after having equilibrated the chain configurations in the total system, we choose the simulation time $t = 0$ and call all chains which have their center of gravity in the left half of the system as A chains, and all chains which have their center of gravity in the right half as B chains. Thus if one labels the coordinate in the long direction as $z = 1,2,...,80$, the distribution function for the center of gravities $\mathbf{R}_g$ of the A chains in the initial state is the step function $\Theta(40 - R_{gz})$. Assuming that the distribution of the effective monomers around the center of gravity is Gaussian, $\phi(\mathbf{r} - \mathbf{R}_g) \sim \exp[-9(\mathbf{r} - \mathbf{R}_g)^2/\langle R^2\rangle]$, where $\langle R^2\rangle$ is the mean square end-to-end distance of the chain, a simple calculation yields the initial concentration profile of the monomers of type A as

$$\phi_A(\mathbf{r}, t = 0) \cong \tfrac{1}{2}\phi \operatorname{erfc}[3(z - 40)/\sqrt{\langle R^2\rangle}]. \tag{12}$$

Figure 5 shows that for the volume fractions of interest Eq. (12) is a reasonable approximation.

If one could assume that interdiffusion is described by a simple diffusion equation with an interdiffusion coefficient D_{int} independent of the volume fraction,

$$\frac{\partial \phi_A(r,t)}{\partial t} = D_{\text{int}} \Delta \phi_A(\mathbf{r}, t), \tag{13}$$

solutions of Eq. (13) would have a similar form as Eq. (12) but with a time-dependent width[51]

$$\phi_A(\mathbf{r}, t) = \tfrac{1}{2}\phi \operatorname{erfc}\left(\frac{z - 40}{2\sqrt{D_{\text{int}} t}}\right),$$

$$\phi_B(\mathbf{r}, t) = \phi\left[1 - \tfrac{1}{2}\operatorname{erfc}\left(\frac{z - 40}{2\sqrt{D_{\text{int}} t}}\right)\right]. \tag{14}$$

Now Eq. (14) obviously involves crude approximations: (i) for $t = 0$ it reduces to the initial condition

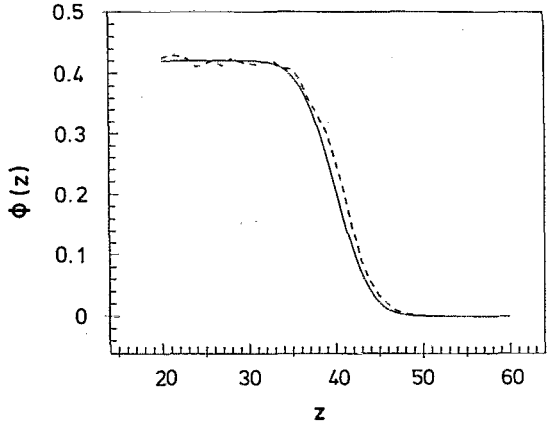

FIG. 5. Density profile of the A chains in the initial configuration for $\phi = 0.42$, $N = 20$ as observed in the simulation (broken curve) and compared to the prediction Eq. (12) (full curve). All simulation results on concentration profiles are obtained from averaging over 48 lattices which are executed in parallel.

$\phi_A(\mathbf{r},t=0)=\phi\Theta(40-z)$ instead of Eq. (12); (ii) since there is reason to expect that the interdiffusion coefficient D_{int} does depend on ϕ, the local volume fraction $\phi_A(\mathbf{r},t)$ is described by a concentration profile expressed by a more complicated functional form.[18] In practice, however, statistical errors of the present simulation seem too large to allow detection of systematic deviations from Eq. (14), see Fig. 6. Therefore we follow the procedure of Ref. 13 (and of the analysis of corresponding experimental data[40]) to extract D_{int} from the interquartile width $W(t)$, which is defined from the distance over which $\phi_A(\mathbf{r},t)$ decays from $3\phi/4$ to $\phi/4$. Using Eq. (14) this yields

$$W(t)=2\beta\sqrt{D_{int}t} \quad \text{with} \quad \beta\approx 0.96, \tag{15}$$

If one would have a profile different from Eq. (14) but also staying invariant with time, Eq. (15) would hold with a somewhat different constant β. Figure 7(a) gives an example of the time dependence of $W(t)$ obtained in our data, and fitting Eq. (15) to such data we obtain the interdiffusion coefficients shown in Fig. 7(b).

Self-diffusion constants are determined from the Einstein relation for the center of gravity of the chains

$$\langle[\mathbf{R}_{cg}(t+t_0)-\mathbf{R}_{cg}(t_0)]^2\rangle=6Dt, \quad t\to\infty. \tag{16}$$

To eliminate slow transients it is useful to plot

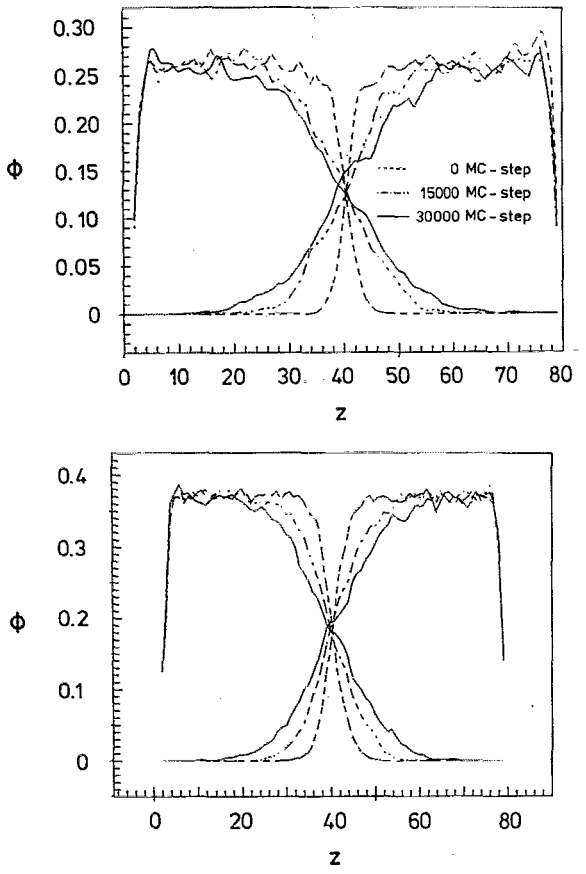

FIG. 6. Density profile of A chains (left) and B chains (right) plotted at three times. (a) $t=0$ (broken curves), $t=1.5\times10^4$ (dash–dotted curves), and $t=3\times10^4$ (full curves), for $N=10$, $\phi=0.262$. (b) $t=0$ (broken curves), $t=3\times10^4$ (dash–dotted curves), $t=10^5$ (full curves), for $N=20$, $\phi=0.317$.

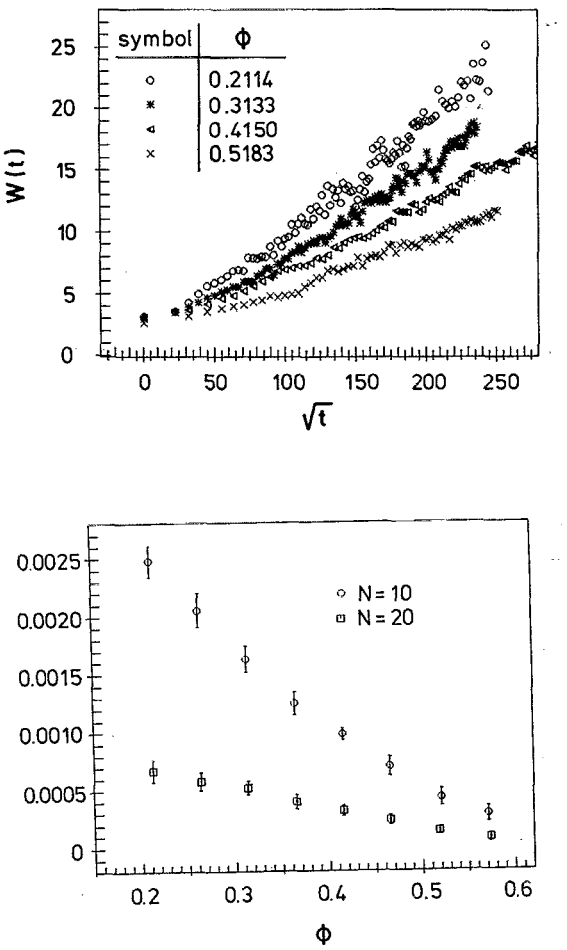

FIG. 7. (a) Interquartile width $W(t)$ plotted vs $\sqrt{t}$ (time being measured in units at attempted Monte Carlo step per monomer) for $N=10$ and four different volume fractions. (b) Interdiffusion coefficients D_{int} for $N=10$ (circles) and $N=20$ (squares) plotted vs ϕ in the athermal case.

$\langle[\mathbf{R}_{cg}(t+t_0)-\mathbf{R}_{cg}(t_0)]^2\rangle/6t$ vs $1/t$ and check whether the data indeed settle down to constants [Fig. 8(a)]. The resulting self-diffusion coefficients are plotted vs ϕ for $N=10$ and $N=20$ in Fig. 8(b). It is seen that again a dramatic slowing down with increasing density occurs. The self-diffusion coefficient of monomers ($N=1$) is shown for comparison [Fig. 8(c)]. Finite size effects are a crucial limitation for determining the self-diffusion coefficients, because on one hand one has to simulate considerably long until the measured coefficients settle down to constant values (up to $\sim$30 h on a CRAY YMP for $N=40$), on the other hand if one includes data from too long times, the traced polymers start to feel the hard walls and one measures diffusion in a confined geometry instead of free diffusion. This effect becomes most important for small chains at low densities. We overcame this problem by tracing only those polymers which initially had their center of masses at least 20 lattice spacings away from either wall. Only the times when the mean square displacement of those polymers was $\leqslant(20-R_{gyr})^2$ were used to determine the self-diffusion coefficients. For the systems considered R_{gyr} ranges from $\approx$3.5 to $\approx$8. The mean square displacements can therefore grow large enough so that the process well reaches the

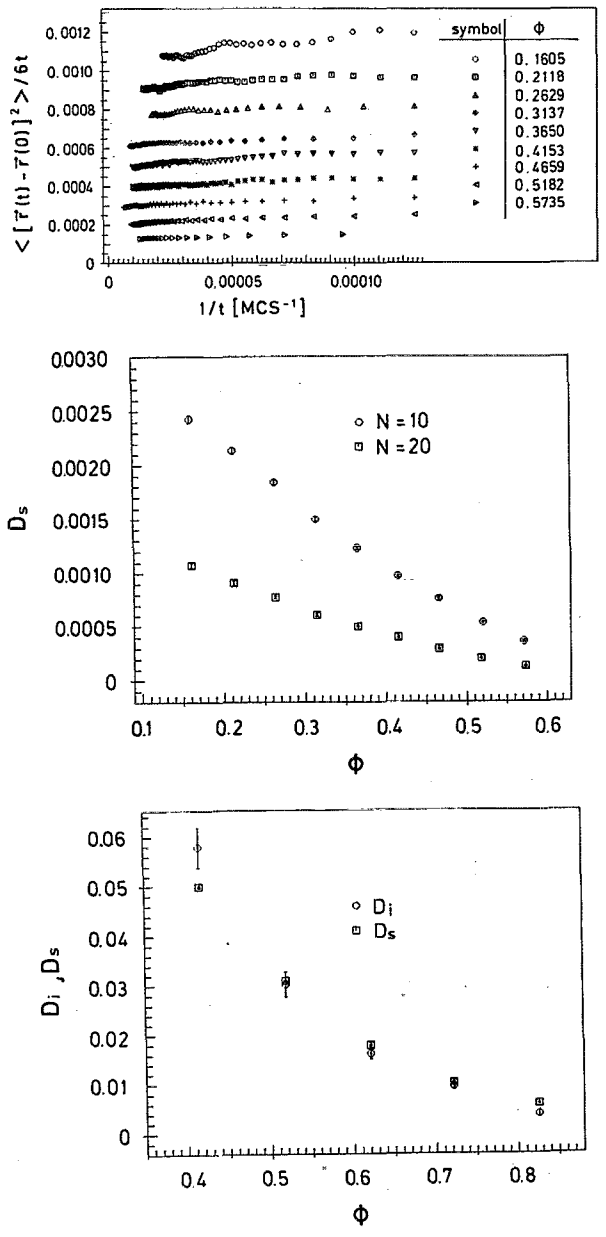

FIG. 8. (a) Mean square displacements of the center of gravity of chains with $N = 20$ bonds divided by the time t plotted vs 1. Different volume fractions are shown as indicated. (b) Self-diffusion coefficients plotted vs density for $N = 10$ (dots) and $N = 20$ (squares). (c) Self-diffusion constant and interdiffusion constant for monomers.

asymptotic regime. Also the window we have chosen the traced polymers from is large enough to provide good statistics. Always several thousand polymers could be used for the average. It is clear that for longer chains than considered here these conditions are no longer fulfilled if the lattice dimension in the z direction is not increased considerably.

One can get an estimate for the statistical error involved if one assumes that the polymer centers follow approximately the distribution $P(\mathbf{r},t) = (4\pi D_s t)^{-1/3} e^{-r^2/4D_s t}$ which is a solution of the diffusion equation $\partial_t P = D_s \Delta P$[r: $= \mathbf{R}_{cg}(t + t_0) - \mathbf{R}_{cg}(t_0)$]. With this distribution one gets as an estimate for the error of $D_s \equiv \lim_{t\to\infty} \langle r^2\rangle/6t$:

$$\Delta D_s = n^{-1/2} \frac{\sqrt{\langle r^4\rangle - \langle r^2\rangle^2}}{6t} = \sqrt{\frac{2}{3n}}\, D_s. \qquad (17)$$

Here n is the number of independent measurements, i.e., the number of traced polymers. Typically this error is around 2%–3%.

Figure 9 now presents a plot of D_{int}/D_{self} vs ϕ in order to test Eq. (11). In view of the large statistical errors (shown by error bars in Fig. 9) and systematic errors, e.g., resulting from a different constant β in Eq. (15) we feel that our data do not indicate important deviations from Eq. (11).

It should be emphasized that for the chain lengths $N = 10$ and $N = 20$ the range of volume fractions covered in Figs. 8(b), 8(c), and 9 covers both the dilute and semidilute regime of concentrations[52] of polymer solutions in a good solvent. As is well known,[52] for dilute solutions the mean square end-to-end distance should behave as $\langle R^2\rangle \sim N^{2\nu}$ with $\nu \approx 0.59$, while for volume fractions ϕ exceeding the overlap concentration ϕ^* (with $\phi^* \sim N^{1-3\nu}$ in three dimensions) the chain radius behaves as $\langle R^2\rangle \sim \phi^{-(2\nu-1)/(3\nu-1)} N \approx \phi^{-0.23} N$. The latter relation which simply follows from requesting that for $\phi \approx \phi^*$ a smooth crossover in the chain linear dimensions occurs, is tested in Fig. 10. It is seen that the concentration dependence of $\langle R^2\rangle$ is consistent with the behavior expected for the semidilute regime over a broad range of volume fractions. Actually volume fractions ϕ in the range $0.4 \lesssim \phi \lesssim 0.6$ already correspond to concentrated polymer solutions and melts; however, in the present model there is no clear-cut distinction between the semidilute and the concentrated solution regime. A more detailed investigation of such scaling concepts[52] appropriate to semidilute solutions requires much larger chain lengths than available in the present work and will be presented elsewhere.[53]

IV. INTERACTION EFFECTS ON INTERDIFFUSION

While all results presented so far refer to the athermal case, this section now considers the effect of an attractive energy ϵ between monomers of different kind. As mentioned in Sec. II, we choose the same interaction energy ϵ for all neighbor distances from the set $\mathbf{P}(2,0,0) \cup \mathbf{P}(2,1,0)$

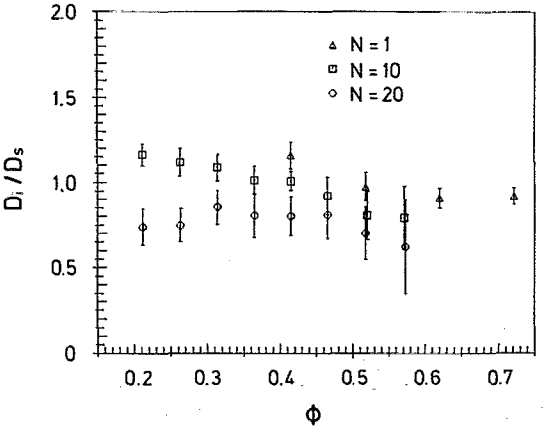

FIG. 9. Ratio of diffusion constants D_{int}/D_{self} for $N = 1$ (triangle), $N = 10$ (squares), and $N = 20$ (dots) plotted as function of the volume fraction ϕ.

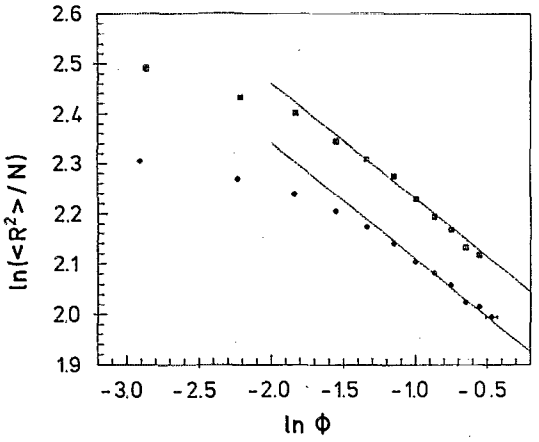

FIG. 10. Log–log plot of normalized mean square end-to-end vector $\langle R^2\rangle/N$ vs ϕ. Straight lines show the theoretical exponent -0.23 (cf. text).

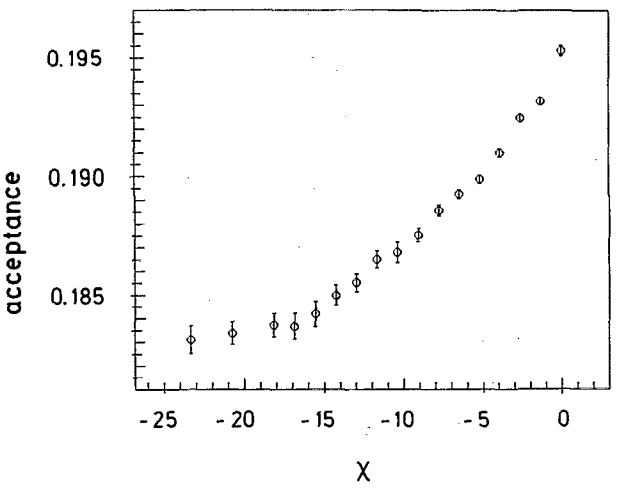

FIG. 11. Acceptance rate R_a plotted vs χ for chains with $N=20, \rho=0.42$ for the initial state ($t=0$) where all A chains have their center of gravity on the left side of $z=40$, and all B chains on the right side of $z=40$. Here $\chi = q\epsilon_{AB}/k_BT$ and $q=14$.

$\cup \mathbf{P}(2,1,1)$. First we wish to make contact with the trandiational Flory–Huggins description of a mixture[54] where the free energy of mixing per lattice site is written as a sum of the entropy of mixing terms and an enthalpy term

$$\frac{F}{k_BT} = \frac{\phi_A \ln \phi_A}{N_A} + \frac{\phi_B \ln \phi_B}{N_B} + \phi_v \ln \phi_v + \chi_{AB}\phi_A\phi_B, \tag{18}$$

where ϕ_A, ϕ_B, and ϕ_v are the volume fractions of lattice sites taken by A monomers, B monomers, and vacant sites, respectively, N_A and N_B are the chain lengths of A chains and B chains, and the Flory–Huggins parameter χ_{AB} accounts for the energy between AB monomers. It can be related to the above energy ϵ in terms of an effective coordination number $q=14$, which is the maximum number of effective monomers that one considered monomer can interact with, for the above choice of the potential range:

$$\chi_{AB} = q\epsilon/(k_BT). \tag{19}$$

However, a naive use of Eq. (19) would yield a slight overestimation of the enthalpy of mixing: two out of the $q\phi_B$ neighbors of a B monomer, which one implies in Eqs. (19) and (18), are typically neighbors along the chemical sequence of the chain, and should not be included in the enthalpy. The number of neighbors of a given monomer belonging to different chains, within the range of interaction, can be estimated by integrating the pair distribution function of Fig. 3. We estimate that for our range of interaction at a density of $\phi = 0.42$ these numbers are

$$p(N=10) \cong 2.70, \quad p(N=20) \cong 2.66,$$
$$p(N=40) \cong 2.64, \tag{20}$$

whereas $q\phi_B = 2.94$ in the region where $\phi_A = \phi_B = \phi/2$.

In order to identify the range of the parameter ϵ/k_BT which is useful for our study we examine the acceptance rate R_a (Fig. 11). Note that only monomers in the interfacial region may have A–B contacts, while elsewhere in the system only A–A contacts and B–B contacts occur, which do not contribute to a change of R_a. It is seen that the acceptance rate saturates when $-\chi$ exceeds values of about 15. Since we wish to stay in the range where the interaction is relatively weak, we restrict attention to the range $0 < -\chi \leqslant 6$. Figure 12(a) shows typical data: it is seen that the concentration profile is qualitatively consistent with the fit to an error function as in the athermal case [Eq. (14)]. However, a very different pattern of behavior results for large values of $|\chi|$, which distinctly exceed the range quoted above, see Fig. 12(b): the strong A–B attraction leads to a polymer density enhancement in the center of the profiles (near $Z=40$), where initially the chance is highest to form A–B "contacts" [i.e., monomer pairs of different type having their distance vectors in the set $\mathbf{P}(2,0,0) \cup \mathbf{P}(2,1,0) \cup \mathbf{P}(2,1,1)$]. However, the formation of this dense central layer of A–B contacts considerably slows down further unmixing: due to the excluded volume constraint, the acceptance rate for any further motion of monomers within this layer is strongly reduced already due to the polymer density enhancement, and it is reduced further since most possible motions would tend to break up some favorable A–B "contacts" and hence have small transition probability w [Eq. (8)]. As a result, this A–B layer with locally enhanced polymer volume fraction in the center of the system acts as a region blocking further unmixing, at least for an intermediate time scale. Of course, this phenomenon is a nonequilibrium effect but it is nevertheless of interest considering that experimentally thin layers of different polymers can be cast onto each other[40] and in the case of strong attractive forces similar effects might occur.

We have restricted the analysis in terms of the interquartile width to weak attractive interactions, of course, because only the concentration profile [Fig. 12(a)] resembles the error function profile found in the athermal case (Fig. 6). From the interquartile widths [Fig. 13(a)] the interdiffusion constants are obtained [Fig. 13(b)] applying Eq. (15) as for the athermal case. It is seen that for weak $|\chi|$ the

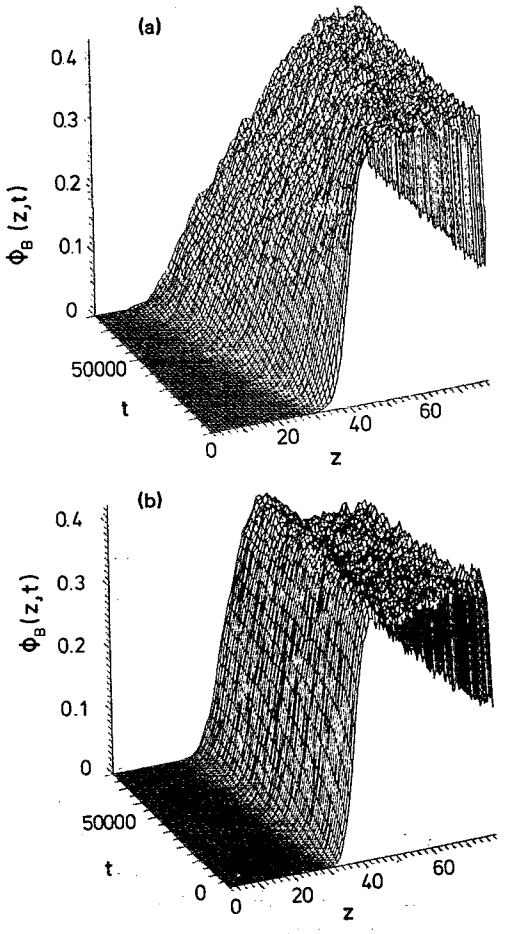

FIG. 12. Time evolution of the concentration profile $\phi_B(z,t)$ for $\phi = 0.42$, $N = 20$, and two choices of the interaction parameter: $\chi = -3.889$ (a) and $\chi = -12.963$ (b).

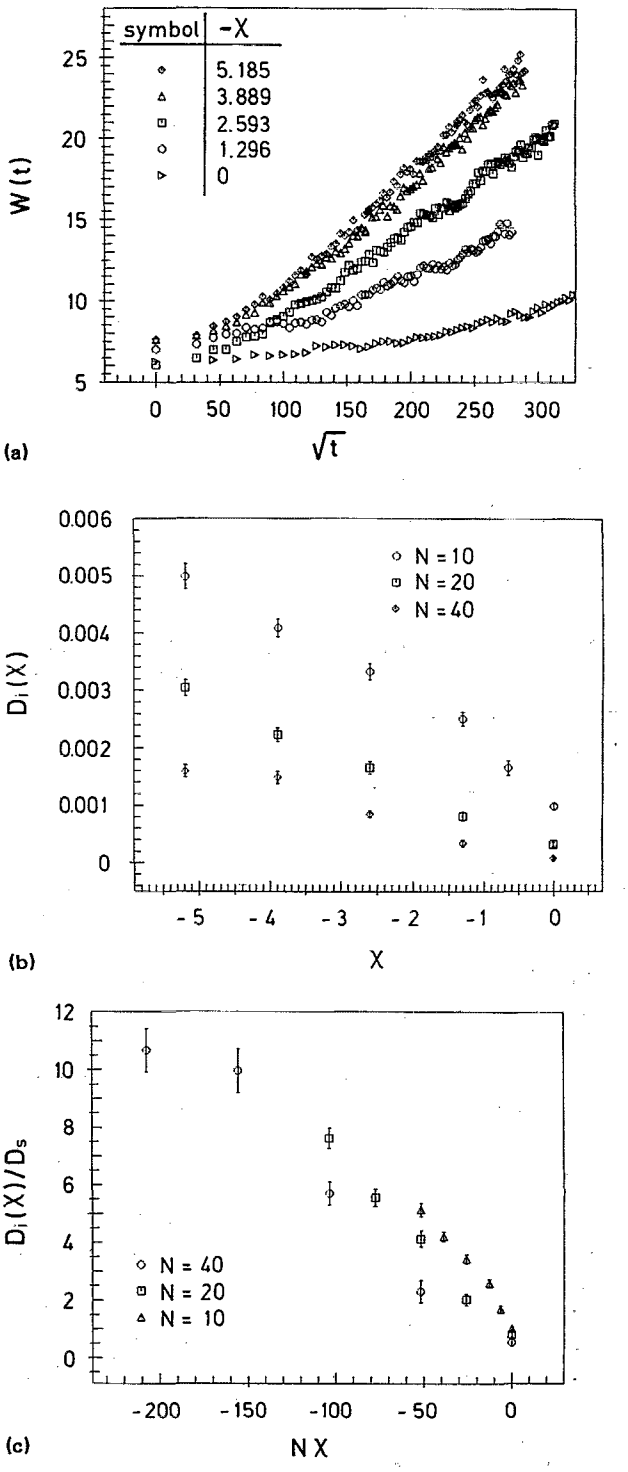

FIG. 13. (a) Time evolution of the interquartile width $W(t)$ for $N = 40$, $\phi = 0.42$ and different choices of χ as indicated in the figure. Note that for $N = 40$ the lattice linear dimensions have been chosen as $30 \times 30 \times 80$, to avoid self-overlap of chains due to periodic b.c. (b) Interdiffusion constant D_{int} plotted vs χ for the three different chain lengths $N = 10$, 20, and 40, respectively. (c) Scaled interdiffusion constant ND_{int} plotted vs scaled interaction parameter $N\chi$, using the data for Fig. 12(b).

interdiffusion constant D_{int} increases with $|\chi|$ linearly, while at larger values of $|\chi|$ the increase is weaker than linear. Since the phenomenological theories[18-20,26] predict

$$D_{\text{int}}(\chi)/D_{\text{int}}(\chi = 0) = 1 - 2\phi_A\phi_B N\chi \qquad (21)$$

we plot $ND_{\text{int}}(\chi)$ vs $N\chi$ in Fig. 13(c) since now all data should fall on a single universal curve, as long as our data are in the Rouse model regime where $D_{\text{int}}(\chi = 0) \sim D_{\text{self}} \sim 1/N$. Since the crossover to reptative behavior sets in around[53] $N \approx 50$ for the present monomer volume fraction $\phi \approx 0.42$, most of the data fall well into this Rouse regime. While for the shortest chain length $N = 10$ one can recognize from Figs. 13(b) and 13(c) some systematic deviations from Eq. (21), the larger chain lengths seem to be compatible with Eq. (21) over a significant range of $N\chi$. For a more discriminating test of Eq. (21) data with much higher precision would be needed, of course, but this would need prohibitively large effort even on computers such as the CRAY-YMP. It should also be remembered that Eq. (21) is derived[13,18-20,26] from a linearization of the interdiffusion equations; therefore it should be better tested with a simulation similar to Ref. 30, where small concentration differences relax rather than studying the highly nonlinear interdiffusion problem as done here. Clearly, such a study also is much more demanding in its statistical needs, and hence has not been attempted.

V. CONCLUDING REMARKS

In this paper, we first have discussed the formulation of the bond fluctuation model on the simple cubic lattice. We have shown that this lattice model is suitable and convenient for the simulation of polymer dynamics in dense polymer systems: with a single type of random motion for the effective monomers (jump by one lattice unit in a randomly chosen lattice direction), one can obtain a Rouse-like behavior of single chains, taking both excluded volume and entanglement restrictions straightforwardly into account. Due to the many choices for the bond vectors joining the effective monomers, the acceptance rate for motions is still reasonably high in rather dense polymer systems, and the lack of ergodicity (which all such lattice models with only local motions have if double accupancy of lattice sites is forbidden[9]) in practice is much less of a problem than for the standard algorithm[3] of Fig. 1(a). Due to the fluctuation in bond lengths and the many choices of angles between adjoining bond vectors, the present model is believed to be a better approximation of a coarse-grained real chain formed by combining a group of $n \approx 3$–6 successive chemical monomers into an "effective monomer" or "Kuhn segment,"[52,54] respectively, than the standard lattice model of Fig. 1(a). In future work this approximate mapping of real polymers on lattice models of the present type will be considered in more detail. As a further motivation why it is desirable to investigate the present algorithm we mention that it is suitable for a generalization to star polymers and general polymer networks, and then the chosen dynamics [Fig. 1(b)] would render the branch points mobile, while in the standard algorithm [Fig. 1(a)] branch points would never move.

An important consideration for the use of such algorithms for computer simulation is the efficiency with which it can be implemented. In the present paper, lattice sizes $20\times20\times80$ (for $N=1,10,20$) and $30\times30\times80$ (for $N=40$) have been studied, running 48 such lattices in parallel. In the athermal case for the $30\times30\times80$ lattice, the number of attempted monomer motions per second is about 7.4×10^5 (including the interaction with 54 neighboring sites, the program gets a factor of about 2.5 slower). These numbers refer to CRAY-YMP. We have also found that the relaxation would be slowed down if larger jump distances for the effective monomers are used, because then the acceptance rate of the attempted motions gets fairly small. In any case, with an effort of a few hours CPU time one can obtain well-equilibrated chain configurations which contain significant information both on static (Fig. 10) and dynamic properties of single chains (Fig. 8). Since we have studied many concentrations ϕ and several choices of the chain length and consider also the fairly slow dynamics of interdiffusion of chains in binary mixtures, via the broadening of the concentration profiles $\phi(z,t)$ altogether an effort of several hundred hours CPU time on vectorizing computers has been spent, and hence it is not straightforward to extend the present study to significantly longer chains.

Our study of interdiffusion has allowed a first check of two predictions of the phenomenological theory: for a symmetric mixture whose both types of chains have the same self-diffusion coefficient D_s, the interdiffusion coefficient $D_{\rm int}$ should be equal to D_s, irrespective of the monomer volume fraction ϕ in the system; for a thermal mixture, with attractive interactions $-\chi>0$ between monomers of different kind, the interdiffusion constant should be enhanced relative to the athermal case, the enhancement being proprotional to χN. Within the albeit rather large statistical errors of our results for $D_{\rm int}$ for various choices of N, χ, and ϕ, we find rough agreement with these predictions. A finding which has not yet predicted by theory, however, is the occurrence of a "blocking layer" of strong A–B contacts in the interface for large values of $|\chi|$. This blocking layer results from a volume fraction enhancement of monomers in the center of the interface, as A monomers move to the right and B monomers move to the left, triggered by their attraction, and "stick" to each other, reducing the possibilities for other monomers to "pass" this layer.

In future work we intend to use the present model to study mixtures with repulsive interactions between different kinds of monomers, which have a miscibility gap. In the framework of our simulation technique, one then can attempt to study the kinetics of the formation of an interface between coexisting phases, a problem which has been studied recently in beautiful experiments[54] and which still poses a lot of theoretical questions.

ACKNOWLEDGMENTS

One of us (H.-P.D.) is supported by the Deutsche Forschungsgemeinschaft (DFG) under Grant No. Bi314/3-1. We are grateful to W. Jilge, I. Carmesin, and K. Kremer for information on details of the program used in Ref. 13. We are particularly indebted to H. P. Wittmann for stimulating discussions helping to develop some of the arguments presented in Sec. II. Thanks also are due to the Höchstleistungsrechenzentrum (HLRZ) Jülich and to the Regionales Hochschulrechenzentrum Kaiserslautern (RHRK) for grants of computer time on the CRAY-YMP and VP 100 vector processors.

[1] M. Doi and S. F. Edwards, *The Theory of Polymer Dynamics* (Clarendon, Oxford, 1986).
[2] For recent reviews, see A. Baumgärtner, in *Applications of the Monte Carlo Method in Statistical Physics*, edited by K. Binder (Springer, Berlin 1984), Chap. 5, and Refs. 3 and 4.
[3] K. Kremer and K. Binder, Comput. Phys. Rep. **7**, 259 (1988).
[4] K. Binder, in *Molecular Level Calculations of the Structures and Properties of Non-Crystalline Polymers*, edited by J. Bicerano (Dekker, New York, in press).
[5] A. Baumgärtner, Annu. Rev. Phys. Chem. **35**, 419 (1984).
[6] K. Kremer, G. S. Grest, and I. Carmesin, Phys. Rev. Lett. **61**, 566 (1988); K. Kremer and G. S. Grest, J. Chem. Phys. **92**, 5057 (1990); see also G. S. Grest and K. Kremer, Phys. Rev. A **33**, 3628 (1986).
[7] P. H. Verdier and W. H. Stockmayer, J. Chem. Phys. **36**, 227 (1962); P. H. Verdier, *ibid.* **45**, 2122 (1966).
[8] H. J. Hilhorst and J. M. Deutch, J. Chem. Phys. **63**, 5153 (1975); M. Boots and J. M. Deutch, *ibid.* **67**, 4608 (1977).
[9] N. Madras and A. Sokal, J. Stat. Phys. **47**, 573 (1987).
[10] K. Kremer, Macromolecules **16**, 1632 (1983).
[11] A. Kolinski, J. Skolnick, and R. Yaris, J. Chem. Phys. **86**, 1567, 7164, 7174 (1987).
[12] I. Carmesin and K. Kremer, Macromolecules **21**, 2819 (1988); in *Polymer Motion in Dense Systems*, edited by D. Richter and T. Springer, Springer Proceedings in Physics, Vol. 29 (Springer, Berlin, 1988), p. 214;

J. Phys. (Paris) **51**, 950 (1990).
[13] W. Jilge, I. Carmesin, K. Kremer, and K. Binder, Macromolecules (in press).
[14] P. E. Rouse, J. Chem. Phys. **21**, 127 (1953).
[15] P. G. de Gennes, J. Chem. Phys. **55**, 571 (1971); Macromolecules **9**, 587 (1976).
[16] For recent reviews, see H. H. Kausch and M. Tirell, Annu. Rev. Mater. Sci. **19**, 341 (1989), and Ref. 17.
[17] K. Binder and H. Sillescu, in *Encyclopedia of Polymer Science and Engineering, Suppl. Volume, 2nd ed.*, edited by J. I. Kroschwitz (Wiley, New York, 1989), p. 297.
[18] F. Brochard, J. Jouffroy, and P. Levinson, Macromolecules **16**, 1638 (1983).
[19] F. Brochard, J. Jouffrey, and P. Levinson, J. Phys. Lett. (Paris) **44**, L-455 (1983).
[20] K. Binder, J. Chem. Phys. **79**, 6387 (1983).
[21] E. J. Kramer, P. Green, and C. Palmstrom, Polymer **25**, 473 (1984).
[22] H. Sillescu, Makromol. Chem. Rapid Commun. **5**, 519 (1984).
[23] F. Brochard and P. G. de Gennes, Europhys. Lett. **1**, 221 (1986).
[24] A. Z. Akcasu, M. Benmouna, and H. Benoit, Polymer **27**, 1935 (1986).
[25] H. Sillescu, Makromol. Chem., Rapid Commun. **8**, 393 (1987).
[26] K. Binder, Colloid Polym. Sci. **265**, 273 (1987).
[27] T. E. Schichtel and K. Binder, Macromolecules **20**, 1671 (1987).
[28] F. C. Brochard-Wyart, F. C. R. Acad. Sci. Ser. II (France) **305**, 657 (1987).
[29] W. Hess and A. Z. Akcasu, J. Phys. (France) **49**, 1261 (1988).
[30] K. W. Kehr, K. Binder, and S. M. Reulein, Phys. Rev. B **39**, 4891 (1989).
[31] P. T. Gilmore, R. Falabella, and R. L. Laurence, Macromolecules **13**, 880 (1980).
[32] R. W. Garbella and J. H. Wendorff, Macromol. Chem., Rapid Commun. **7**, 591 (1986).
[33] R. A. L. Jones, J. Klein, and A. M. Donald, Nature **321**, 161 (1986).
[34] R. J. Composto, J. W. Mayer, E. J. Kramer, and D. White, Phys. Rev. Lett. **57**, 1312 (1986).
[35] U. Murschall, E. W. Fischer, Ch. Herkt-Maetzky, and G. Fytas, J. Polym. Sci., Polym. Lett. Ed. **24**, 191 (1986).
[36] R. J. Composto, E. J. Kramer, and D. M. White, Nature **328**, 234 (1987).
[37] M. G. Brereton, E. W. Fischer, G. Fytas, and U. Murschall, J. Chem. Phys. **87**, 5048 (1987).
[38] G. Fytas, Macromolecules **20**, 1430 (1987).
[39] J. Kanetakis and G. Fytas, J. Chem. Phys. **87**, 5048 (1987).
[40] A. E. Jordan, R. C. Ball, A. M. Donald, L. J. Fetters, R. A. L. Jones, and J. Klein, Macromolecules **21**, 235 (1988).
[41] J. Baschnagel, W. Paul, and K. Binder (in preparation).
[42] The argument presented here can be found in a more elaborate form in H.-P. Deutsch, Dissertation, Universität Mainz, 1991 (in preparation). We are deeply indebted for very useful discussions to H.-P. Wittmann, which helped clarify this derivation.
[43] N. Metropolis, A. W. Rosenbluth, M. N. Rosenbluth, A. H. Teller, and E. Teller, J. Chem. Phys. **21**, 1087 (1953).
[44] A. Sariban and K. Binder, Macromolecules **21**, 711 (1988).
[45] K. Binder, Colloid Polym. Sci. **266**, 871 (1988).
[46] H.-P. Deutsch, Dissertation, Universität Mainz, 1991 (in preparation).
[47] C. P. Flynn, *Point Defects and Diffusion* (Clarendon, Oxford, 1972).
[48] J. R. Manning, *Diffusion Kinetics for Atoms in Crystals* (Van Nostrand, Princeton, 1968).
[49] E. Howard and A. B. Lidiard, Rep. Progr. Phys. **27**, 161 (1964); A. R. Allnatt and A. B. Lidiard, *ibid.* **50**, 373 (1987).
[50] K. W. Kehr and K. Binder, in *Applications of the Monte Carlo Method in Statistical Physics*, edited by K. Binder (Springer, New York, 1987), p. 181.
[51] M. Abramowitz and I. A. Stegun, *Handbood of Mathematical Functions* (Dover, New York, 1965).
[52] P. G. de Gennes, *Scaling Principles of Polymer Physics* (Cornell University, Ithaca, 1979).
[53] W. Paul, K. Binder, D. W. Heermann, and K. Kremer, J. Phys. (Paris) (in press).
[54] P. J. Flory, *Principles of Polymer Chemistry* (Cornell University, Ithaca, N.Y., 1953).
[55] U. Steiner, G. Krausch, G. Schatz, and J. Klein, Phys. Rev. Lett. **64**, 1119 (1990).